
HOKKAIDO UNIVERSITY

Title	Paleoceanographic changes in the Eastern Equatorial Pacific over the last 10 Myr
Author(s)	Seki, Osamu; Schmidt, Daniela N.; Schouten, Stefan; Hopmans, Ellen C.; Damsté, Jaap S. Sinninghe; Pancost, Richard D.
Citation	Paleoceanography, 27(3), PA3224 https://doi.org/10.1029/2011PA002158
Issue Date	2012-09-01
Doc URL	http://hdl.handle.net/2115/52111
Rights	©2012 American Geophysical Union
Type	article
File Information	Pal27_PA3224.pdf


Instructions for use

Hokkaido University Collection of Scholarly and Academic Papers : HUSCAP

Paleoceanographic changes in the Eastern Equatorial Pacific over the last 10 Myr

Osamu Seki,[1,2] Daniela N. Schmidt,[3] Stefan Schouten,[4] Ellen C. Hopmans,[4] Jaap S. Sinninghe Damsté,[4] and Richard D. Pancost[1]

Received 25 April 2011; revised 1 July 2012; accepted 10 July 2012; published 1 September 2012.

[1] To examine the Late Neogene evolution of tropical Pacific oceanography, we determined multiple geochemical proxy records for temperature ($U^{K'}_{37}$ and TEX^{H}_{86} indices) and primary productivity (algal biomarkers and diol indices) in sediments recovered at ODP Site 1241 in the East Equatorial Pacific (EEP) spanning a record of the last 10 Myr. The TEX^{H}_{86} temperatures are lower than those recorded by $U^{K'}_{37}$ indices, exhibiting large fluctuations and suggesting strong warming during the Mid Pliocene Warm Period (MPWP; 4.5–3.2 Ma) and significantly colder temperature during the Late Miocene cooling period (7–5 Ma) and after the Middle Pliocene Warm Period (MPWP). Such variations could reflect changes in the EEP thermocline temperatures, but we suggest that they instead reflect changes in the depth of export production of glycerol dialkyl glycerol tetraether lipids in response to changes in the upper ocean structure. A combination of temperature records, inferred to represent different and likely varying depths in the water column, as well as algal biomarker records for export production and ecosystem structure, suggest that both productivity and inference upwelling were reduced in the EEP during warmer periods, such as the MPWP and prior to 7 Ma. In contrast, stronger upwelling conditions and associated increased productivity likely prevailed from 7 to 5 Ma and for the past 3 Myr, both corresponding to globally cool intervals. A further increase in EEP productivity occurred at ca 1.8 Ma, coincident with the development of the E-W Pacific SST gradient. These results confirm previous work that protracted El Niño–like conditions prevailed during warmer intervals of the Pliocene before ultimately descending into the current climate state.

Citation: Seki, O., D. N. Schmidt, S. Schouten, E. C. Hopmans, J. S. Sinninghe Damsté, and R. D. Pancost (2012), Paleoceanographic changes in the Eastern Equatorial Pacific over the last 10 Myr, *Paleoceanography*, *27*, PA3224, doi:10.1029/2011PA002158.

1. Introduction

[2] The tropical Pacific Ocean provides a substantial portion of the atmosphere's sensible and latent heat making it a central driver of our global climate. The heat transport is influenced by the thermal structure of the upper water column which, in the Pacific Ocean, is affected by the El Niño and La Niña oceanographic modes of the El Niño–Southern Oscillation (ENSO) [*Cane*, 1998]. During El Niño years, Eastern Equatorial Pacific (EEP) upwelling is dramatically reduced, resulting in a less pronounced vertical temperature gradient and lower primary productivity in the EEP and a less pronounced longitudinal sea surface temperature (SST) gradient compared to non-El Niño years. The Intergovernmental Panel on Climate Change Fourth Assessment Report (IPCC AR4) anticipates future tropical Pacific climate change that has been described as El Niño–like [*Meehl et al.*, 2007]. El Niño conditions cause a reduction of precipitation in Northern Australia, Southeast Asia and Africa and flooding in countries along the Andes, making it important to understand the link between global climate, ENSO and the Pacific thermal structure.

[3] Several paleoceanographic studies suggest dramatic changes in the tropical Pacific Ocean during the climate transitions over the past 6 Myr. In particular, the warm Pliocene (3.2–4.5 Ma), the most recent period of sustained global warmth associated with elevated pCO_2, has been argued to be associated with both protracted El Niño–like [e.g., *Wara et al.*, 2005] and La Niña–like [e.g., *Rickaby and Halloran*, 2005] conditions. Sea surface temperature records in the tropical Pacific (ODP Sites 806, 846, 847 and 1241)

[1]Organic Geochemistry Unit, Cabot Institute and Bristol Biogeochemistry Research Centre, School of Chemistry, University of Bristol, Bristol, UK.
[2]Now at Institute of Low Temperature Science, Hokkaido University, Sapporo, Japan.
[3]School of Earth Sciences, University of Bristol, Bristol, UK.
[4]Department of Marine Organic Biogeochemistry, NIOZ Royal Netherlands Institute for Sea Research, Den Burg, Netherlands.

Corresponding author: O. Seki, Institute of Low Temperature Science, Hokkaido University, N19W8 Kita-ku, Sapporo, Hokkaido 060-0819, Japan. (seki@pop.lowtem.hokudai.ac.jp)

©2012. American Geophysical Union. All Rights Reserved.
0883-8305/12/2011PA002158

based on foraminiferal Mg/Ca ratios and $U^{K'}_{37}$ indices suggest that aspects of the early Pliocene climate resembled the present-day pattern associated with El Niño events, with warmer SST in the EEP and a reduced west-east temperature gradient [*Wara et al.*, 2005; *Lawrence et al.*, 2006; *Ravelo et al.*, 2006; *Dekens et al.*, 2007; *Steph et al.*, 2010]. These authors suggested that during the Pliocene, El Niño–like conditions were a protracted rather than an interannual phenomenon. Importantly, the relationship to long-term ($>10^6$ years) global climate change is unclear due to the diachrony of climate change between the tropics and high latitudes [*Ravelo et al.*, 2004]. A further complication is the uncertainty in the applicability of Mg/Ca and $U^{K'}_{37}$ temperature proxies to long-term temperature reconstructions [*Medina-Elizalde et al.*, 2008], and additional temperature records are therefore useful.

[4] Most previous studies on El Niño–like phenomena have focused on only the final intensification of Northern Hemisphere Glaciation (NHG) during the middle Pliocene and the Mid-Pleistocene Transition (MPT). However, a major step in NHG started during the Miocene around 7 Ma [*Thiede et al.*, 1998; *Lear et al.*, 2003; *Fronval and Jansen*, 1996; *Vidal et al.*, 2002]. Therefore, we investigate the thermal history of the eastern equatorial Pacific over the past 10 Myr in order to better understand late Miocene and Pliocene oceanographic conditions in the EEP. We analyzed two paleotemperature proxies in sediments recovered at ODP Site 1241: the relatively new TEX_{86} temperature proxy based on the number of cyclopentyl moieties in the glycerol dialkyl glycerol tetraether (GDGT) lipids of pelagic Thaumarchaeota [*Schouten et al.*, 2002; *Kim et al.*, 2010] and alkenone-derived $U^{K'}_{37}$ indices. For the former, these represent the first long-term Neogene data. We compare these new records to published foraminiferal Mg/Ca ratios [*Wara et al.*, 2005; *Rickaby and Halloran*, 2005; *Steph et al.*, 2006; *Groeneveld et al.*, 2006], and consider the potential evolution of the Mg/Ca ratio of seawater (see also Data Set S1 in the auxiliary material).[1] As an independent line of evidence for changes in oceanography, we measured algal biomarker-based paleoproductivity proxies that could also be indicative of upwelling intensity [*Rampen et al.*, 2008].

2. Materials and Methods

2.1. Samples

[5] The sediments for our study were obtained from ODP Site 1241A located on the Cocos Ridge in the Guatemala Basin of the EEP (5°50′N, 86°26′W; 2027 m water depth). Although today ODP Site 1241 is out of the upwelling center (Figure 1), an El Niño still induces an increase of SST by as much as ~3°C with associated decreases in primary productivity [*Wang and Fiedler*, 2006]. A tectonic backtrack of the Cocos plate shows that ODP Site 1241 was located further south, closer to the equatorial divergence during the late Miocene and Pliocene epoch [*Mix et al.*, 2003], a change which must be taken into account when interpreting our data (Figure 1). Moreover, geological data suggest that the intertropical convergence zone prior to the Pliocene was further north compared to its present position [*Hovan*, 1995]. The age model of ODP Site 1241 is mainly determined by linear interpolation between biostratigraphic datums [*Mix et al.*, 2003; *Flores et al.*, 2006]. Additionally, the ages in the critical time interval between 5.8 and 2.5 Ma are based on orbital tuning of the benthic foraminiferal oxygen isotope ($\delta^{18}O$) record [*Tiedemann et al.*, 2006].

2.2. Biomarker Concentrations and Distributions

[6] Organic matter in homogenized freeze-dried sediment was saponified with 0.3 M KOH for 2 h. Total lipids were then extracted from sediments by ultrasonication (10 min) using, sequentially, methanol, dichloromethane/methanol (2:1, v/v) and dichloromethane. The extracts were separated into neutral and acid fractions using liquid/liquid separation, and the neutral fraction was further separated into four fractions (aliphatic hydrocarbons, aromatic hydrocarbons, alkenones and alcohols) by silica gel column chromatography (230–400 mesh). Alkenones were analyzed via gas chromatography (HP5890 GC equipped with an on-column injector, CPSIL-5CB fused silica capillary column, 50 m × 0.32 mm inner diameter, film thickness of 0.25 mm) and flame ionization detector, whereas C_{28}-1,14- and C_{30}-1,15-diols were measured via gas chromatography/mass spectrometry (Thermo Trace GC/MS), with both quantified using an internal standard (C_{19} *n*-alkanol). The alcohol fraction was silylated with *N*,*O*-bis-(trimethylsilyl)trifluoroacetamide (BSTFA) to analyze the diols as their trimethylsilyl (TMS) ether derivatives. The GC oven temperature was programmed from 50°C to 120°C at 30°C/min and then 120°C to 310°C at 5°C/min. The analytical reproducibility of the $U^{K'}_{37}$ temperature values is about ±0.2°C, whereas the calibration error (±1 s.d.) is 1.5°C [*Conte et al.*, 2006].

[7] Analysis of GDGTs was performed according to *Schouten et al.* [2007] using an HP 1100 series liquid chromatograph/mass spectrometer equipped with auto-injector. Separation was achieved with Prevail Cyano column (2.1 × 150 mm, 3 μm; Alltech, Deerfield, IL, USA). Detection was achieved using atmospheric pressure positive ion chemical ionization mass spectrometry (APCI-MS) of the eluent. The reproducibility of the TEX^H_{86} values, based on analytical limitations, is typically 0.01, which is equivalent to ±0.3°C [*Schouten et al.*, 2007], whereas the calibration error is about 2.5°C [*Kim et al.*, 2010].

2.2.1. $U^{K'}_{37}$ Derived Temperature

[8] $U^{K'}_{37}$ indices in sediments were converted into growth temperatures using the calibration equation:

$$T = \left(U^{K'}_{37} - 0.044\right)/0.033 \quad (1)$$

which was established from the global core top calibration [*Müller et al.*, 1998]. Previous comparisons of $U^{K'}_{37}$ temperatures in surface sediments and in situ annual mean temperatures indicate that maximum production of alkenones is in the surface mixed layer of the ocean [e.g., *Prahl et al.*, 2006], such that $U^{K'}_{37}$-derived temperature reconstructions reflect surface mixed layer temperature in the EEP region. Moreover, there is no evidence that sedimentary $U^{K'}_{37}$-SST records are substantially biased by factors such as changes in haptophyte ecology and species of dominant producer over the past several Myr [*Lawrence et al.*, 2006; *Dekens et al.*, 2007]. However, some work suggests that the

[1] Auxiliary materials are available at ftp://ftp.agu.org/apend/pa/2011pa002158/.

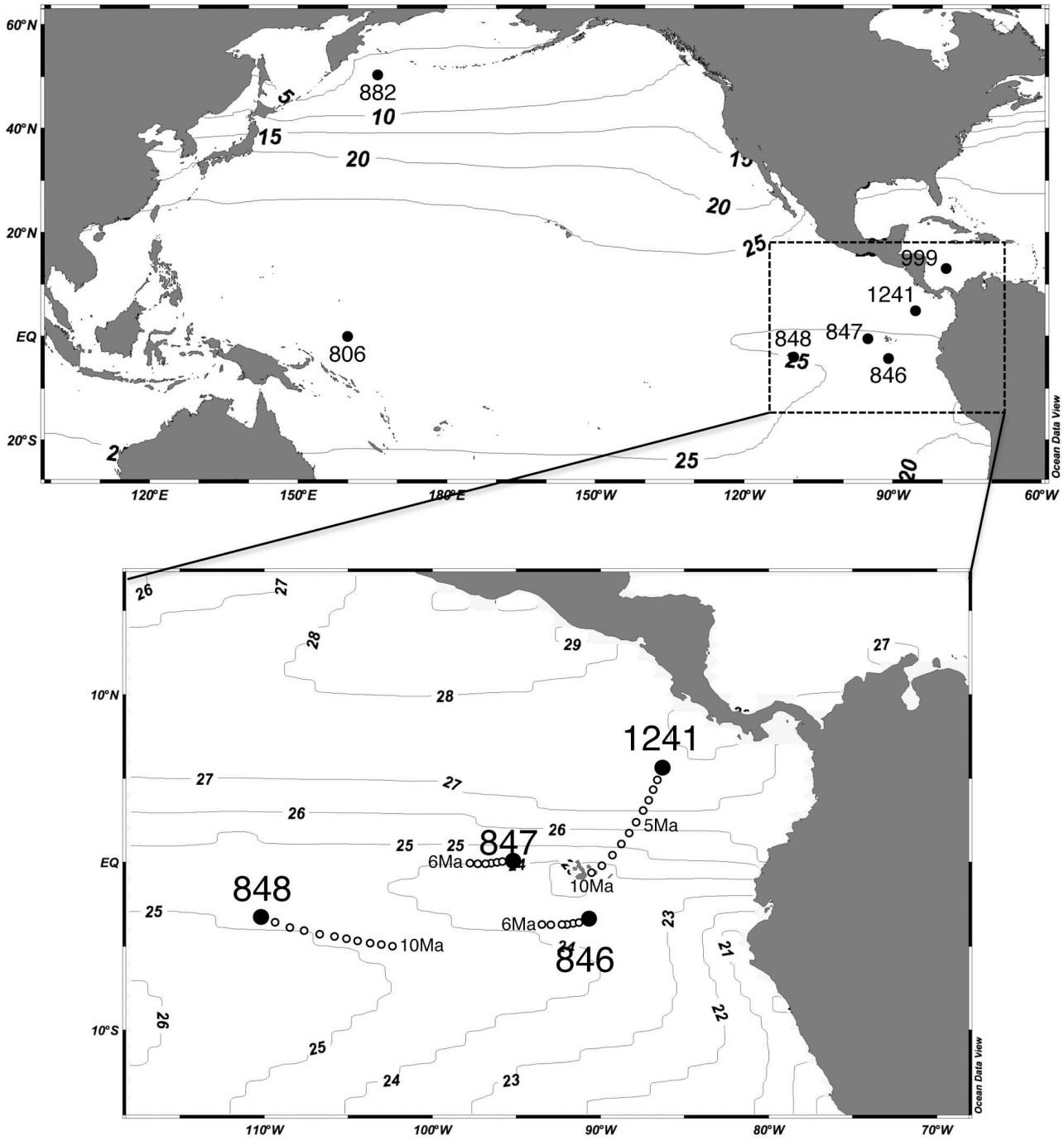

Figure 1. Modern annual mean SST in the Pacific Ocean from the World Ocean Atlas 2005 [*Locarnini et al.*, 2006]. (top) The solid circles represent the current locations of ODP Sites 846, 847, 848, 882, 999 and 1241. (bottom) Open circles represent positions of Sites 846, 847 and 1241 for the past 10 Myr (in 1 million year steps) [*Farrell et al.*, 1995; *Mix et al.*, 2003]. Tectonic movement of the Coccos plate shifted the site location ~950 km to the northeast toward its modern position [*Mix et al.*, 2003].

relationship between $U^{K'}_{37}$ and alkenone production temperature is nonlinear (less sensitive) above SSTs > 24°C [*Sonzogni et al.*, 1997; *Conte et al.*, 2006] and has an upper limit of 27–28°C [*Conte et al.*, 2006]. Because modern (and presumably Pliocene) annual mean SSTs in the EEP are >24°C (Figure 2), it is possible that $U^{K'}_{37}$ values provide minimum SST values during parts of our record if actual SSTs were >28°C.

2.2.2. TEX^{H}_{86} Derived Temperature

[9] Isoprenoid GDGTs containing cyclopentyl moieties in marine environments are biosynthesized mainly by ammonia-oxidizing marine Thaumarchaeota [*de la Torre et al.*, 2008;

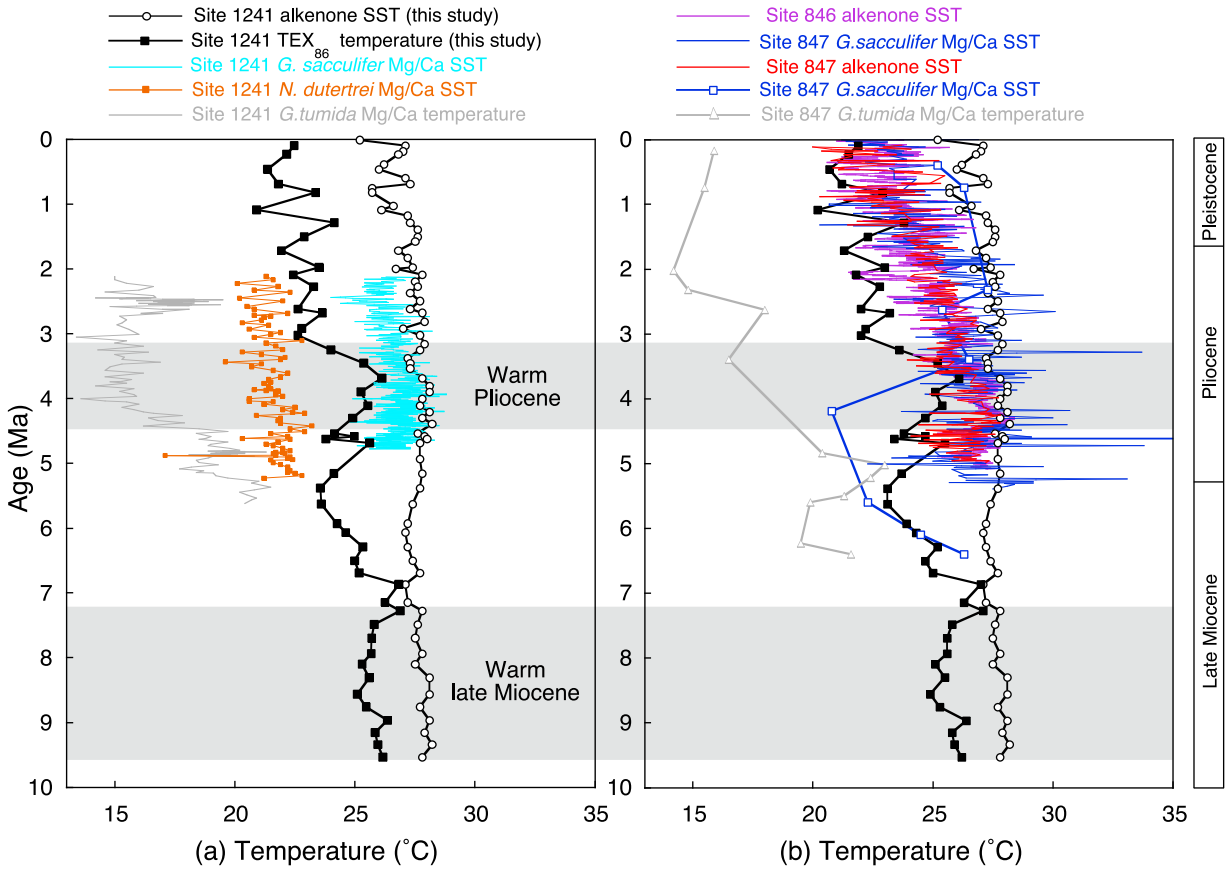

Figure 2. $U^{K'}_{37}$ and TEX^{H}_{86} temperatures in ODP Site 1241 and previously published Plio-Pleistocene temperature records from the tropical Pacific. (a) The black open circle represents $U^{K'}_{37}$ SSTs in ODP Site 1241; the black solid square represents TEX_{86} temperature in ODP Site 1241; the blue line represents *G. sacculifer* Mg/Ca SSTs at ODP Site 1241 [*Groeneveld et al.*, 2006]; the brown solid square represents *N. dutertrei* Mg/Ca temperature at ODP Site 1241 [*Steph et al.*, 2006]; the gray line represents G. tumida Mg/Ca temperature at ODP Site 1241 [*Steph et al.*, 2006]. (b) The purple line represents $U^{K'}_{37}$ SSTs at ODP Site 846 [*Lawrence et al.*, 2006]; the blue line represents *G. sacculifer* Mg/Ca SSTs at ODP Site 847 [*Wara et al.*, 2005]; blue open squares represent *G. sacculifer* Mg/Ca SSTs at ODP Site 847 [*Rickaby and Halloran*, 2005]; the red line represents $U^{K'}_{37}$ SSTs at ODP Site 847 [*Dekens et al.*, 2007]; the gray open triangles represent *G. tumida* Mg/Ca temperatures at ODP Site 847 [*Rickaby and Halloran*, 2005]. $U^{K'}_{37}$ (black open circle) and TEX^{H}_{86} (black solid square) temperatures in ODP Site 1241 are superimposed on Figure 2b for a comparison with temperature records in other sites.

Schouten et al., 2008; *Pitcher et al.*, 2010] and are ubiquitous in marine sediments [*Schouten et al.*, 2002; *Kim et al.*, 2010]; they are also widespread in soils, albeit at lower relative concentrations [*Weijers et al.*, 2006]. The TEX^{H}_{86} is defined [*Kim et al.*, 2010] as:

$$TEX^{H}_{86} = \log[(GDGT2 + GDGT3 + Crenarchaeol\text{–}isomer) / (GDGT1 + GDGT2 + GDGT3 + Crenarchaeol\text{-}isomer)] \quad (2)$$

and TEX^{H}_{86} values were converted to temperatures using the calibration equation:

$$T = 68.4 * TEX^{H}_{86} + 38.6 \quad (r^2 = 0.87, n = 255) \quad (3)$$

which was derived from a global core top calibration of marine surface sediments with surface temperatures [*Kim et al.*, 2010] and has a calibration error of 2.5°C. It has been suggested that the marine GDGT signal can be biased by the input of terrestrial GDGTs [*Weijers et al.*, 2006]. Such inputs can be evaluated using the branched isoprenoid index (BIT), which is an indicator of the relative contribution of soil-derived branched (non-isoprenoidal) GDGTs to marine GDGTs [*Hopmans et al.*, 2004]. A terrigenous bias of TEX^{H}_{86} values has been suggested to be limited to those sediments where BIT indices are >0.3 [*Weijers et al.*, 2006], but BIT indices at ODP Site 1241 range between 0.02 and 0.14, and most values are lower than 0.05.

2.3. Temperature Calculations From Mg/Ca Ratios

[10] In this study, we reconstruct temperatures using previously reported Mg/Ca ratios from three foraminiferal species (*Globigerinoides sacculifer* without its sacc-like final chamber, *Neogloboquadrina dutertrei* and *Globorotalia*

tumida). Different habitats among these species allows reconstruction of temperatures at different depths: in the EEP, *G. sacculifer* lives in surface mixed layers, *N. dutertrei* dwells at shallow thermocline depths (30–50 m), and *G. tumida* lives at the bottom of the photic zone (below ~80–100 m depth) [*Fairbanks et al.*, 1982; *Ravelo and Fairbanks*, 1992]. We have compiled previously published *G. sacculifer* Mg/Ca records from ODP Sites 847 and 1241 [*Wara et al.*, 2005; *Rickaby and Halloran*, 2005; *Groeneveld et al.*, 2006]; all have been converted to growth temperatures using the equation of *Dekens et al.* [2002] as follows:

$$\mathrm{Mg/Ca} = 0.37\exp 0.09[\text{temperature} - 0.36(\text{depth in km}) - 2.0^{\circ}\mathrm{C}] \quad (4)$$

[11] Previously published *N. dutertrei* Mg/Ca ratios [*Steph et al.*, 2006] were converted into temperature by using equation (5) for Atlantic *N. dutertrei* rather than the Pacific, Ontong Java based, calibration by *Dekens et al.* [2002]. This is because in most ODP Site 1241 samples, *N. dutertrei* temperatures estimated by using the Pacific calibration exceed the *G. sacculifer* derived temperatures. This result conflicts with the fact that *N. dutertrei* lives in the subsurface and *G. sacculifer* lives in the warm surface mixed layer [*Steph et al.*, 2006, and references therein]. This is corroborated by the raw δ^{18}O values of *N. dutertrei* which are much higher than those of *G. sacculifer* in ODP Site 1241 during the Pliocene [*Steph et al.*, 2006], confirming that that the former lived in the cooler subsurface environment. The Atlantic correction used is:

$$\mathrm{Mg/Ca} = 0.60\exp 0.08[\text{temperature} - 2.8(\text{depth in km})] \quad (5)$$

These equations take account of the depth-based dissolution effect. Equation (6) [*Anand et al.*, 2003] was used to calculate *G. tumida* Mg/Ca temperatures at ODP Sites 847 and 1241 [*Rickaby and Halloran*, 2005; *Steph et al.*, 2006]:

$$\mathrm{Mg/Ca} = 0.38\exp 0.09[\text{temperature}] \quad (6)$$

Because the species-specific dissolution correction of Mg/Ca for *G. tumida* has not been established for the Pacific and *G. tumida* is resistant to dissolution, we did not correct for this.

[12] Reconstruction of temperature by Mg/Ca paleothermometry using the above equations rests on the assumption that the Mg/Ca ratio in seawater has remained constant over the time scale of investigation. However, several studies suggest that seawater Mg/Ca ratios have varied over the past several Myr [e.g., *Wilkinson and Algeo*, 1989; *Stanley and Hardie*, 1998; *Fantle and DePaolo*, 2005, 2006, 2007]. Recently, *Medina-Elizalde et al.* [2008] revised *G. sacculifer* Mg/Ca temperatures in ODP 806 and 847 (initially published by *Wara et al.* [2005]) by adjusting for inferred changes in the Mg/Ca ratio of seawater. In order to explore its potential impact on the *G. sacculifer*, *N. dutertrei* and *G. tumida* Mg/Ca temperature records at ODP Site 1241, we apply a similar adjustment. As with *Medina-Elizalde et al.* [2008], we use seawater Mg/Ca ratios inferred from δ^{44}Ca values of $CaCO_3$ in a sediment from Pacific Ocean [*Fantle and DePaolo*, 2005, 2006] because this provides a Mg/Ca record with a resolution of ~500 kyr (Figure 3c). The δ^{44}Ca record of *Fantle and DePaolo* [2005] is consistent with other δ^{44}Ca records from the Pacific and Indian Oceans [*Heuser et al.*, 2005; *Fantle and DePaolo*, 2007; *Griffith et al.*, 2008] but not the North Atlantic record of *Sime et al.* [2007] (Figure 3c). Estimates of seawater Mg/Ca ratios based on other approaches [*Wilkinson and Algeo*, 1989; *Stanley and Hardie*, 1998; *Horita et al.*, 2002; *Coggon et al.*, 2010] have a lower temporal resolution (Figure 3b) but also suggest that seawater Mg/Ca values at 5 Ma are lower than the present value. However, it should be noted that those agreements do not validate the higher resolution variations, because residence times of Ca and Mg in the ocean are about 1 and 22 Ma, respectively. Therefore, shorter-term variations should be interpreted with caution. It is important to note, that this correction introduces large discrepancies between SST proxies [e.g., *Dekens et al.*, 2007].

[13] The detailed procedure of the correction is described in *Medina-Elizalde et al.* [2008] and references cited therein. Briefly, modeled seawater Mg/Ca values are reconstructed based on δ^{44}Ca values of $CaCO_3$ in a sediment core (Figure 3b) [*Fantle and DePaolo*, 2005, 2006]. To account for past Mg/Ca variability, the pre-exponential constants in equations 1, 2 and 3 are adjusted by a factor equal to the percentage difference between seawater Mg/Ca from a given age and modern seawater Mg/Ca [*Fantle and DePaolo*, 2006]. Second, the partition coefficient between calcite and seawater has been adjusted to take into consideration that the Mg partition coefficient in calcite increases as the Mg/Ca ratio decreases in seawater [*Mucci and Morse*, 1983], using the relationship derived from inorganic calcite precipitation [*Mucci and Morse*, 1983]. We note that given the issues discussed above, the reconstructed changes in seawater Mg/Ca of *Fantle and DePaolo* [2006] remain the subject of much controversy; in particular the limited number of data, both spatially and temporally, in that study limit the applicability and could give rise to significant errors in temperature reconstructions. Thus, we use these revised records primarily to explore the uncertainty in existing Mg/Ca based temperature records.

2.4. Biomarker Productivity Indicators

[14] Long-chain C_{37} alkenones derive exclusively from haptophyte algae [*Conte et al.*, 1994], specifically the *reticulofenestrids.* The C_{28}-alkyl-1,14-diol occurs in diatoms of the genus *Proboscia* [*Sinninghe Damsté et al.*, 2003], a species associated with upwelling conditions [*Koning et al.*, 2001] and a marine heterokont alga *Aprdinella radians* which is predominant in estuarine waters [*Rampen et al.*, 2011]. Since these biomarkers are characteristic of certain microalgae, they can be used as qualitative proxies for the reconstruction of past phytoplankton export production. Even though diagenetic effects prevent quantitative assessment of biomarker source input, down-core profiles of their concentration and mass accumulation rates (MAR) can be used to reconstruct variations in marine primary productivity [e.g., *Seki et al.*, 2004; *Lawrence et al.*, 2006; *Dekens et al.*, 2007; *Rampen et al.*, 2008]. Hence, we converted the

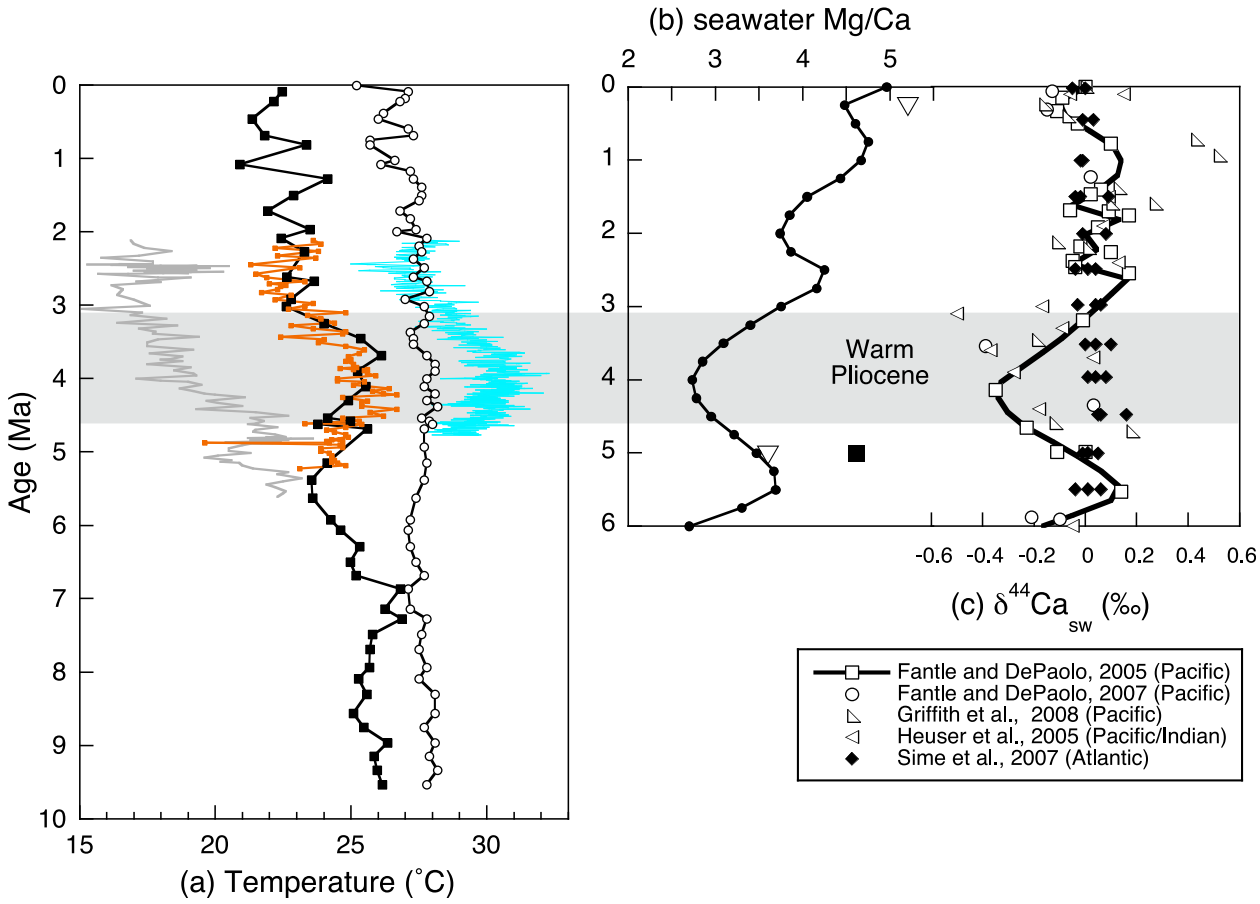

Figure 3. (a) TEX_{86}^{H}, $U_{37}^{K'}$ temperature and the adjusted Mg/Ca temperatures records at ODP Site 1241 together with seawater Mg/Ca change over the last 10 Myr. Black open circles represent $U_{37}^{K'}$ SSTs at Site 1241; black solid squares represent TEX_{86}^{H} temperatures at ODP Site 1241; blue line represents adjusted *G. sacculifer* Mg/Ca SSTs in ODP Site 1241; brown square represents adjusted *N. dutertrei* Mg/Ca subsurface temperature; gray line represents adjusted *G. tumida* Mg/Ca subsurface temperature in ODP Site 1241. (b) Seawater Mg/Ca reconstructions by δ^{44}Ca [*Fantle and DePaolo*, 2006] (solid circles) and halite-trapped fluid inclusions (open triangle [*Horita et al.*, 2002] and solid square [*Lowenstein et al.*, 2001]). (c) The δ^{44}Ca records in bulk carbonate [*Fantle and DePaolo*, 2005, 2007], marine barite [*Griffith et al.*, 2008] and planktonic foraminifera [*Heuser et al.*, 2005; *Sime et al.*, 2007]. In Figure 3c, open symbols represent Pacific and Indian Ocean samples while solid diamond shows Atlantic Ocean samples. Bold line in Figure 3c represents an interpolation curve of *Fantle and DePaolo* [2005] data.

concentrations of algal biomarkers to MARs using the following equation:

$$\mathrm{MAR}(\mathrm{g/cm^2/kyr}) = \mathrm{DBD}(\mathrm{g/cm^3}) \times \mathrm{LSR}(\mathrm{cm/kyr}) \times \mathrm{concentration}(\mu\mathrm{g/g}) \quad (7)$$

where DBD and LSR are dry bulk density and linear sedimentation rate, respectively.

[15] We also employ the diol index, the ratio of [C_{28} 1,14-diol]/{[C_{28} 1,14-diol] + [C_{30}-1,15-diol]} [*Rampen et al.*, 2008], to reconstruct changes in nutrient level associated with eastern Tropical Pacific upwelling. The biological sources for C_{30}-1,15-diols are still unclear but include eustigmatophyte microalgae [*Volkman et al.*, 1992; *Méjanelle et al.*, 2003; *Rampen et al.*, 2007]. Because *Proboscia* diatoms are especially abundant in nutrient-rich regions such as upwelling areas [*Koning et al.*, 2001], whereas C_{30}-1,15-diol producers are widespread, high diol indices have been proposed to be high productivity and upwelling indicators [*Rampen et al.*, 2008]. A particular advantage of the diol index is that it is the ratio of two compounds with similar chemical structures and potentially similar degradation rates, such that it is unlikely altered by diagenetic reactions in the sediment.

3. Results

3.1. Temperature Records

[16] At ODP site 1241, $U_{37}^{K'}$ SSTs range from 25 to 28°C over the past 10 Myr and were at least 27 to 28°C throughout the Pliocene and late Miocene (Figure 2). A slight cooling from 28 to ~26°C occurred during the Pleistocene, although sampling resolution was insufficient to examine the range of glacial-interglacial variability. As the global core top calibration indicates that the $U_{37}^{K'}$ proxy could deviate from

linearity at temperatures higher than 26°C [*Conte et al.*, 2006], our data suggest that EEP SST has been at least warmer than 27–28°C in the Pliocene and Miocene.

[17] In general, $U^{K'}_{37}$ SSTs at ODP Site 1241 during the Pliocene match the $U^{K'}_{37}$ temperatures at Site 847 [*Dekens et al.*, 2007] but are consistently slightly higher (~1°C) than the *G. sacculifer* Mg/Ca SSTs at ODP Sites 847 and 1241 [*Wara et al.*, 2005; *Groeneveld et al.*, 2006] (Figure 2a). Considering analytical uncertainties of both SST methods, this difference is insignificant during the Pliocene. However, the Plio-Pleistocene cooling recorded at ODP Site 1241 is less than the ~3.5°C cooling recorded by $U^{K'}_{37}$ indices and Mg/Ca ratios at Sites 846 and 847 (Figure 2b).

[18] In contrast to the $U^{K'}_{37}$ SSTs, TEX^{H}_{86} temperatures at ODP Site 1241 exhibit large fluctuations, from 21° to 27°C over the past 10 Myr with significant stepwise cooling from ~7 to 5.5 Ma and ~3.5 to 3 Ma and a warm reversal between 5 and 3.7 Ma (Figure 2a). These temperatures are up to 5°C lower than $U^{K'}_{37}$ SSTs at ODP Site 1241, a difference much larger than the analytical uncertainties of both methods (0.2 and 0.3°C for $U^{K'}_{37}$ and TEX^{H}_{86} temperatures, respectively) and the proxy-SST calibration errors (1.5 and 2.5°C for $U^{K'}_{37}$ and TEX^{H}_{86} temperatures, respectively). The temporal TEX^{H}_{86} temperature trend also differs from those derived from $U^{K'}_{37}$ indices and the *G. sacculifer*, *N. dutertrei* and *G. tumida* Mg/Ca ratios [*Steph et al.*, 2006], with the TEX^{H}_{86} temperatures being similar to those determined for the thermocline dwelling *N. dutertrei* in some intervals and similar to the mixed layer *G. sacculifer* in others.

[19] The *G. sacculifer* Mg/Ca SSTs from ODP Site 1241 [*Groeneveld et al.*, 2006] range from 26 to 28°C and are slightly lower than $U^{K'}_{37}$ SSTs (Figure 2a). *N. dutertrei* Mg/Ca temperatures [*Steph et al.*, 2006] exhibit a temporal trend similar to that of *G. sacculifer* Mg/Ca temperatures, though the estimated temperatures are much lower than that of *G. sacculifer.* On the other hand, *G. tumida* Mg/Ca temperatures, indicative of temperatures at the bottom of the thermocline, range from 15 to 21°C at ODP Sites 1241 between 5.5 and 2.1 Ma. Its temporal variation is different from all other temperature records. A strong cooling is recorded at the beginning of the warm Pliocene (4.5 Ma; Figure 2a) and relatively lower temperatures persist until 3 Ma.

[20] Adjustment of seawater Mg/Ca ratios based on the method of *Medina-Elizalde et al.* [2008] yields warmer *G. sacculifer* SSTs in ODP Sites 847 and 1241, especially for the warm Pliocene (29–31°C), compared to the unadjusted records and today (Figure 3a). They also suggest strong warming during the onset of the MPWP (5–4.5 Ma) and then cooling during the transition out of the MPWP at the final NHG (3.5–2.7 Ma). The remarkable warming in the warm Pliocene observed in the TEX^{H}_{86} record is also apparent in adjusted *N. dutertrei* Mg/Ca temperatures. We note, however, that the significantly warmer temperatures in the warm Pliocene arise primarily from the lighter δ^{44}Ca values that are used for reconstruction of seawater Mg/Ca ratios [*Fantle and DePaolo*, 2005, 2006] (Figure 3b).

3.2. Mass Accumulation Rates of Algal Biomarkers and Diol Index

[21] MARs of C_{37} alkenones range from 0.2 to 36 μg/cm^2/kyr over the past 10 Myr while that of the C_{28}-1,14-diol varies between 0 and 20 ng/cm^2/kyr (Figures 4a and 4b). At ODP Site 1241 alkenone MARs are considerably higher, for example, than MARs observed for sediments from the Caribbean Sea spanning the same time interval (ODP Sites 999 and 1000; 0.1 to 8 ng/cm^2/kyr [*Seki et al.*, 2010]). Alkenone MARs at Site 1241 are relatively high during the Late Miocene, but after 5 Ma they are relatively low, except for two isolated peaks at 2.2 and 1.8 Ma. In contrast, alkenone concentrations and MARs at Site 846 and 847 are generally elevated between 3 to 1.5 Ma [*Lawrence et al.*, 2006; *Dekens et al.*, 2007] (Figure 4d). The C_{28}-1,14-diol MAR has a somewhat different record. The C_{28}-1,14 diol MARs are low from 9 to 7 Ma, high but variable from 7 to 4.5 Ma, low again from 4.5 to 3 Ma and higher again from 3 Ma to the present (Figure 4b). The diol indices range from 0 to 0.15 over the last 10 Myr (Figure 4c) again higher than values observed in the Caribbean records (typically 0 to 0.05; O. Seki and R. D. Pancost, unpublished data, 2012). The temporal variations are similar to those of C_{28}-1,14-diol MARs, being relatively high from 7 to 4.5 Ma and from 3 Ma to the present.

4. Discussion

4.1. EEP Temperature Records

[22] The $U^{K'}_{37}$ indices and unadjusted *G. sacculifer* Mg/Ca ratios all record a modest long-term sea surface cooling at ODP Site 1241. The cooling of $U^{K'}_{37}$ SST is smaller than that recorded by comparable records from elsewhere in the EEP (e.g., Site 847; Figure 2b), and long-term SST change at ODP Site 1241 is likely ameliorated compared to these other sites by a combination of the more distal position within the upwelling zone and its northeastward drift since 10 Ma (which would result in a SST increase of ~4°C under modern conditions; Figure 1). Thus, the surface cooling at ODP Site 1241 could be subdued due to the northeastward migration of ODP Site 1241 out of the central upwelling region [*Steph et al.*, 2006]. This change in SST may be regarded as the null hypothesis for oceanographic changes associated with the plate tectonic backtrack path of ODP Site 1241, and significant deviations from this are assumed to reflect temporal changes in regional oceanography that are not related to plate tectonic drift.

[23] The TEX^{H}_{86} temperatures at ODP Site 1241 are lower than corresponding $U^{K'}_{37}$ and unadjusted *G. sacculifer* Mg/Ca-derived SSTs. This discrepancy could either reflect differences in seasonal production or in the depth habitat between alkenone- and GDGT-producers. There is only a small present-day seasonal SST range (2°C) at ODP Site 1241 [*Locarnini et al.*, 2006], and therefore GDGT distributions are likely recording a deeper water temperature signal. This is entirely plausible, given that Thaumarchaeota live throughout the water column [e.g., *Karner et al.*, 2001], and TEX^{H}_{86} likely records the depth of GDGT export. *Ho et al.* [2011] showed that TEX^{H}_{86}-derived temperatures in tropical Pacific Ocean surface sediments correspond to the modern thermocline temperature of 30–50 m rather than SSTs, for a range of different overlying thermal structures (WPWP, mid-tropics, the EEP cold tongue and doldrums). Other studies have shown that in some settings a subsurface water signal is recorded by TEX^{H}_{86}, for example in the Santa Barbara Basin [*Huguet et al.*, 2007], the Benguela upwelling

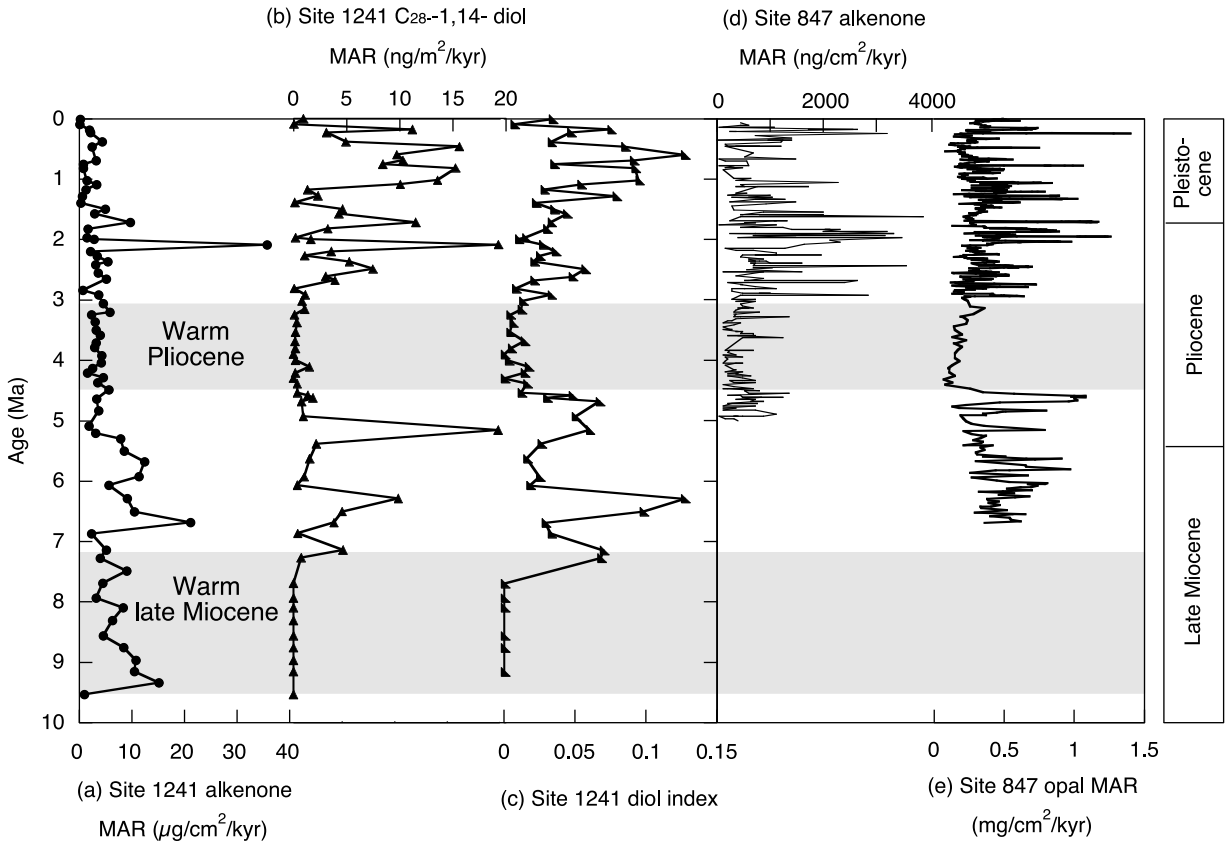

Figure 4. Productivity reconstructions from ODP Sites 1241 and 847 over the past 10 Myr. Mass accumulation rates (MAR) of (a) C_{37} alkenones, (b) C_{28}-1,14-diols, (c) diol indices at Site 1241, and MARs of (d) C_{37} alkenones [*Dekens et al.*, 2007], (e) biogenic opal [*Farrell et al.*, 1995] at Site 847. Note that alkenone MARs at ODP Site 847 were originally published as mg cm^{-1} kyr^{-1}, but that was a misprint and should be reported as ng cm^{-1} kyr^{-1} (P. Dekens, personal communication, 2012).

area [*Lee et al.*, 2008] and the west coast of Africa [*Lopes dos Santos et al.*, 2010]. Thus, low TEX_{86}^{H} values in the equatorial Pacific likely reflect subsurface (approximately 30–50 m) temperatures, possibly due to a deep chlorophyll maximum and associated formation of ammonium, the source of energy for pelagic Thaumarchaeota [e.g., *Könneke et al.*, 2005; *Wuchter et al.*, 2006].

[24] With respect to trends in the TEX_{86}^{H} temperature record, we also must consider the influence of oceanographic change by plate tectonic drift; as with SST, the subsurface temperature (at 50 m water depth) also reflects the 4°C monotonic cooling trend over the past 10 Myr. Unlike the $U_{37}^{K'}$ indices, TEX_{86}^{H} values exhibit an overall cooling of 4°C (albeit interrupted by large fluctuations from the late Miocene to the present), suggesting that the TEX_{86}^{H} temperature record is not related to the paleodrift. Thus, we suggest that TEX_{86}^{H} does record oceanographic change, and in particular thermocline cooling, over the past 10 Myr. However, the temporal variations in the TEX_{86}^{H} temperature record are significantly different from the corresponding Mg/Ca temperature record of the thermocline dwelling *N. dutertrei* (as well as *G. sacculifer* and alkenone-derived records).

[25] There are a number of possible explanations for the different trends. First, it could reflect changes in the depth of GDGT export production over the past 10 Myr. For example, from 4.8 to 3.5 Ma GDGTs could have been exported predominantly from the surface mixed layer yielding TEX_{86}^{H} temperatures similar to those of *G. sacculifer*, whereas from 3.5 Ma to the present, GDGTs were exported from the thermocline, yielding TEX_{86}^{H} temperatures similar to those recorded by *G. dutertrei.* As mentioned above, TEX_{86}^{H} temperatures in surface sediments are lower than those of the overlying surface waters in a variety of modern Pacific Ocean regimes (WPWP, mid-tropics, the EEP cold tongue and doldrums), suggesting that the export depth for the TEX_{86}^{H} signal is presently relatively stable [*Ho et al.*, 2011]. However, other oceanographic regimes suggest that GDGT distributions in sediments tend to reflect a subsurface signal in upwelling regions and a surface signal in non-upwelling regions [*Huguet et al.*, 2007; *Lee et al.*, 2008], suggesting that changes in upwelling regime can affect the export depth of GDGTs. In fact, intervals characterized by relatively low TEX_{86}^{H} temperatures (7–4.5 Ma and 3–0 Ma) are also characterized by relatively high algal biomarker fluxes and vice versa (10–7 Ma and 4.5–3 Ma) (Figure 4), suggesting a close relationship between productivity – and hence upwelling intensity – and the depth of GDGT export and, therefore, TEX_{86}^{H} signatures.

[26] An alternative explanation for the difference between TEX_{86}^{H} and *N. dutertrei* derived temperature trends is that seawater Mg/Ca ratios have varied in the past [*Medina-*

Elizalde et al., 2008; *Medina-Elizalde and Lea*, 2010]. It is widely recognized that seawater Mg/Ca ratios have changed on million year timescales, but the importance of such changes in the Plio-Pleistocene context remains the subject of debate [*Fantle and DePaolo*, 2005, 2006]. At Site 847 in the East Pacific [*Wara et al.*, 2005; *Dekens et al.*, 2007], Plio-Pleistocene $U^{K'}_{37}$ and Mg/Ca derived temperature records are similar, although we note that the former are near their maximum. In contrast, in both the Caribbean Sea [*Steph et al.*, 2010; *Seki et al.*, 2010] and North Atlantic [*Bartoli et al.*, 2005; *Lawrence et al.*, 2009], $U^{K'}_{37}$-derived SSTs are higher than those derived from Mg/Ca ratios from 4.5 to 2.5 Ma in Caribbean Sea and from 2.5 to 3.3 in the North Atlantic. The new data presented in this paper will not resolve that controversy, but an exploration of its impact on reconstructed temperatures is necessary to interpret our organic temperature proxies ($U^{K'}_{37}$ for surface and TEX^{H}_{86} for subsurface thermocline). It is noteworthy that the TEX^{H}_{86} temperature record is markedly similar to temperature records derived from seawater-adjusted *G. sacculifer* and *N. dutertrei* Mg/Ca ratios (albeit 5°C lower than the former), and all exhibit remarkable warming from 5 to 4.5 Ma and subsequent cooling from 3.5 to 3 Ma (Figure 3a). However, warmer Mg/Ca records during the warm Pliocene basically arose from only a single δ^{44}Ca data point in the Mg/Ca seawater correction. It is worth noting though, that other δ^{44}Ca records also show a decrease in δ^{44}Ca values during the warm Pliocene [*Heuser et al.*, 2005; *Fantle and DePaolo*, 2007; *Griffith et al.*, 2008] (Figure 3b). A relatively low seawater Mg/Ca value has also been determined for the Pliocene using halite-trapped fluid inclusions, although this is also limited to a single Pliocene determination [*Horita et al.*, 2002] (Figure 3b). However, it should be noted that a δ^{44}Ca record from the North Atlantic does not show significant changes in δ^{44}Ca values over the past 5 Ma, suggesting no substantial change in seawater Mg/Ca during the period [*Sime et al.*, 2007]. Thus, although most δ^{44}Ca records indicate that seawater Mg/Ca ratios during the warm Pliocene were lower, the estimates still have a relatively large uncertainty [*Sime et al.*, 2007].

[27] With respect to SSTs, the adjusted *G. sacculifer* Mg/Ca SSTs (30–31°C) during the warm Pliocene are significantly higher than $U^{K'}_{37}$-derived SSTs (27–28°C), whereas the difference in unadjusted *G. sacculifer* and $U^{K'}_{37}$ SSTs is insignificant (Figures 2 and 3). This discrepancy might be explained by the 'saturation' of $U^{K'}_{37}$ paleothermometer above 28°C and hence a potential underestimation of the real temperature [*Conte et al.*, 2006]. Moreover, the warmer tropical sea surface temperatures derived from adjusted Mg/Ca ratios (>30°C) are in good agreement with HadCM3 model simulations [*Haywood and Valdes*, 2004; *Haywood et al.*, 2005, 2007; *Lunt et al.*, 2008, 2010] that indicate that high tropical SSTs are required to maintain the Pliocene global warmth when pCO_2 is 400 ppm [*Pagani et al.*, 2010; *Seki et al.*, 2010]. We note, however, that many of these simulations also fail to generate a reduced West to East Pacific SST gradient, and much work remains to rationalize proxy and model data.

[28] We cannot distinguish these two interpretations and conclude that the TEX^{H}_{86} temperature record reflects either (1) migration of GDGT producers between the thermocline and surface waters or (2) strictly a thermocline signal with the implication that the *Medina-Elizalde et al.* [2008] treatment is at least partially valid. Clearly, this work highlights the necessity to revisit and improve our understanding of how the Mg/Ca ratio of seawater has changed through geological time. Different treatments of the Mg/Ca data yield markedly different records, comparison to organic proxy data is non-conclusive, and the modeling of the Ca^{2+} content of seawater from δ^{44}Ca has large uncertainty [*Sime et al.*, 2007]. Of course, paleoceanographic interpretations are possible despite this ongoing debate. Interpretations based on the difference between Mg/Ca records remain largely robust [e.g., *Wara et al.*, 2005; *Groeneveld et al.*, 2006; *Steph et al.*, 2006]. And regardless of interpretation, our biomarker records clearly show dramatic changes in the upper ocean thermal structure in the EEP over the past 10 Myr, and these are discussed below.

4.2. EEP Productivity Records

[29] The alkenone MARs at ODP Site 1241 are much lower and do not match the temporal trends of alkenone MARs at ODP Site 847 over the past 5 Myr (Figure 4a), nor do they match other biogenic ($CaCO_3$, TOC and opal) MARs at Site 847 [*Farrell et al.*, 1995; *Dekens et al.*, 2007] (Figure 4e; $CaCO_3$ and TOC are not shown). Specifically, generally elevated MARs between 3 Ma and the present at Site 847 are not apparent at ODP Site 1241. The difference could arise from the lower sampling resolution of our study or reflect paleodrift of ODP Site 1241 from the upwelling center to a less intense upwelling area. However, neither of these explanations accounts for the fact that diol-based proxies do record increased diatom productivity over the past 3 Myr (Figures 4b and 4c), opposite to the haptophyte proxies (Figure 4a). In fact, the C_{28}-1,14-diol MAR and diol index records at Site 1241 are similar to that of the ODP Site 847 biogenic opal MAR (Figure 4e), also indicative of diatom productivity, over the past 6 Myr.

[30] Diatoms are opportunistic species that are more sensitive to nutrient supply than haptophytes and hence outcompete them in nutrient-rich environments, such that the latter dominate in oligotrophic conditions and the former dominate in upwelling systems [e.g., *Margalef*, 1978; *Ziveri and Thunell*, 2000]. Thus, the increase in diatom biomarkers relative to those from haptophytes over the past 3 Myr at Site 1241 is consistent with increased upwelling and productivity. Although our sampling resolution limits interpretation, it appears that these productivity increases occurred in two stages. First, diatom productivity increased at ca. 3 Ma, with both 1,14-diol MARs and diol indices becoming high and variable, probably on glacial-interglacial timescales. A second increase then apparently occurred between 1.8 and 1.5 Ma reflected particularly by diol indices.

[31] It remains unclear why ODP Site 847 does not show similar patterns of competition between the two phytoplankton groups. Model results suggest that primary productivity at Site 1241 is today limited by silicic acid availability in the surface water, while at Site 847 iron limitation is the main influence on productivity [*Moore et al.*, 2004]; this may have allowed haptophytes to exploit changes in Plio-Pleistocene nutrient status at Site 847, whereas diatoms at ODP Site 1241 could have preferentially benefited from relief of silica limitation. Alternatively, the difference between the two sites could arise from the fact

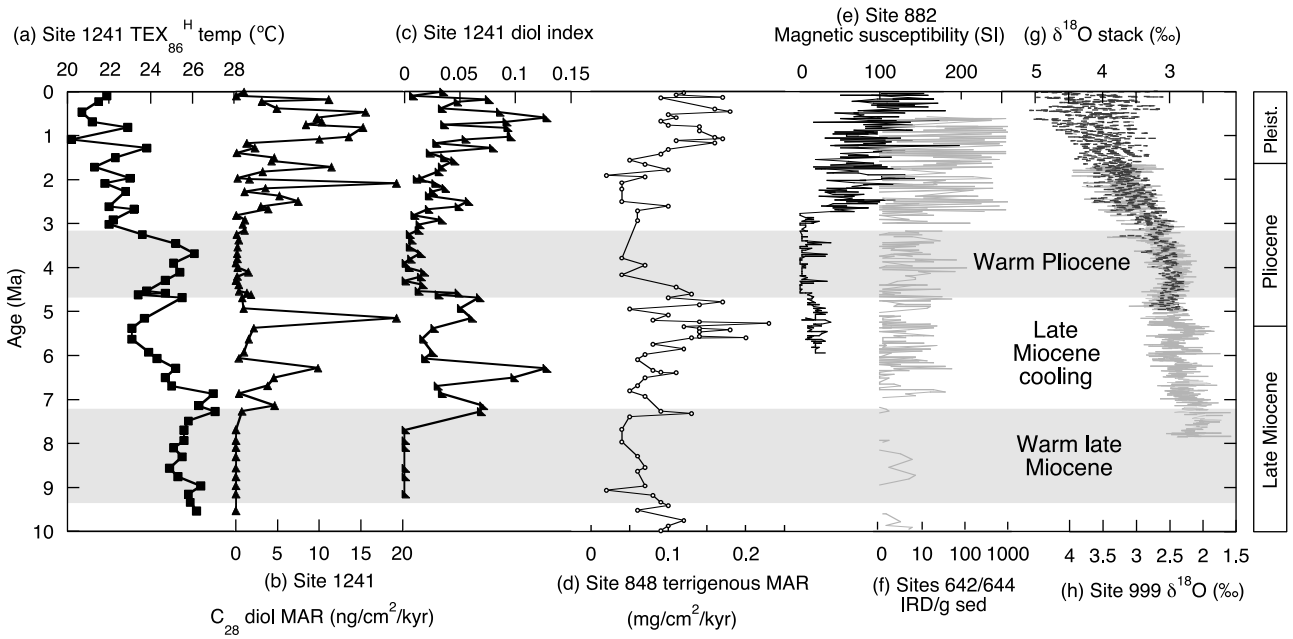

Figure 5. Temperature and productivity reconstructions from Site 1241 and related ODP sites over the past 10 Myr together with high latitude climate records. (a) TEX_{86}^{H} temperature record in ODP Site 1241. (b) Mass accumulation rates (MAR) of C_{28}-1,14-diol at ODP Site 1241. (c) Diol indices at ODP Site 1241. (d) Aeolian MAR in ODP Site 847 [*Hovan*, 1995], reflecting strength of trade wind. (e) Magnetic susceptibility record from Subarctic Pacific ODP Site 882 [*Haug et al.*, 1995] reflecting ice-rafted debris (IRD) input to sediments. (f) IRD record from Norwegian Sea ODP Site 642/644 [*Fronval and Jansen*, 1996]. The benthic foraminiferal oxygen isotope ($\delta^{18}O$) record of high latitude climate change from (g) global stack between 5 and 0 Ma [*Lisiecki and Raymo*, 2005] and (h) Caribbean Sea ODP Site 999 between 7.9 and 1.6 Ma [*Bickert et al.*, 2004].

that ODP Site 1241 is outside the main upwelling area, with the influence of upwelling being more confined to deeper waters. The *Proboscia* diatoms from which C_{28}-1,14-diols derive are early bloom colonizers and have greatest concentrations near the thermocline, where nutrient concentrations are highest [*Koning et al.*, 2001]. In contrast, alkenone-producers live in the mixed layer with the highest productivity and hence the lowest nutrient concentrations. The surface waters could have been limited in nutrients, whereas thermocline waters may have had enough silicic acid to support diatom growth. Thus, the ODP Site 1241 records complement and support the interpretations derived from ODP Site 847 for diatoms, but reveal complexity in the response of the entire phytoplankton community.

4.3. The Evolution of the Upper Ocean in the EEP and at Site 1241

[32] The combination of TEX_{86}^{H} temperature and algal biomarker MARs at ODP Site 1241 (and elsewhere in the EEP) reveals long-term changes in the EEP upper ocean since the late Miocene. In general, the TEX_{86}^{H} temperature record exhibits a long-term cooling trend from the late Miocene to the present, although its interpretation remains challenging, particularly when compared to different Mg/Ca temperature reconstructions. The $U_{37}^{K'}$ indices record a more subtle cooling over the same interval. Biomarker accumulation rates are variable, and diatom and haptophyte biomarkers exhibit markedly different trends. However, diatom productivity indicators, which have been shown to relate well with upwelling intensity [*Rampen et al.*, 2008], are similar, at least for the past 7 Myr, to those obtained from Site 847 (Figure 4). They also coincide with changes in dust accumulation (Figure 5d), supporting a long-term connection between wind strength and elevated productivity in the east Pacific [*Farrell et al.*, 1995; *Diester-Haass et al.*, 2006].

[33] In addition, our records indicate that high productivity intervals coincide with times when TEX_{86}^{H} derived temperatures are low, whereas low productivity intervals coincide with high TEX_{86}^{H} values (Figures 5a–5c). This has important implications for interpretation of all GDGT-derived temperature records as it provides further evidence for a connection between the upper water column thermal structure and TEX_{86}^{H}-derived temperatures [e.g., *Lopes dos Santos et al.*, 2010; *Ho et al.*, 2011]; however, the causal mechanism is unclear as discussed above.

[34] Before about 7.5 Ma, biomarker accumulation rates and diol indices were low, despite a paleoceanographic position closer to the EEP cold tongue, and TEX_{86}^{H} temperatures were high and similar to those observed in the warm Pliocene.

[35] Afterwards, conditions similar in some respects to those of today appear to have dominated. From 6.5 to 5 Ma, although $U_{37}^{K'}$ temperatures at ODP Site 1241 remained high, the difference between TEX_{86}^{H} temperatures and SST proxies began to increase. From 7.5 to 4.5 Ma, biomarker productivity indicators were elevated, in agreement with opal MARs at Site 847 (Figure 4e) and corresponding to increasing aridity and dust accumulation in the North and

South Pacific (e.g., Figure 5d) [*Hovan*, 1995; *Rea*, 1994; *Rea et al.*, 1998]. Hence, the productivity regime in this part of the EEP from 7 to 5 Ma was similar to that of Pleistocene; the TEX_{86} subsurface temperatures were somewhat similar to that of today, albeit not as cold. Our results are generally consistent with the sedimentary record from the Western Pacific Warm Pool (ODP site 806) [*Nathan and Leckie*, 2009], which suggests that the WEP thermal structure and productivity resembled modern El-Niño conditions before 6.5 Ma and modern La Niña conditions after 6.5 Ma. However, our $U^{K'}_{37}$ SST data shows that the zonal SST difference (~2°C) from 7 to 5 Ma was smaller than the modern La Niña condition (~5°C), suggesting that the tropical climate state at that time was not like modern strong La Niña conditions. Less pronounced cooling in surface waters at the end of Miocene could have been due to warmer upwelling water as suggested by the *G. tumida* Mg/Ca temperatures [*Steph et al.*, 2006]. Crucially, ODP Site 1241 biomarker records suggest that the late Miocene conditions did not persist into the Pliocene warm period. From 4.5 to 3.2 Ma, biomarker accumulation rates and diol indices suggest lower productivity, and the high TEX^{H}_{86} temperatures are similar to those observed prior to 7 Ma and markedly different from those observed today. These interpretations are largely consistent with the interpretation of *Wara et al.* [2005], *Lawrence et al.* [2006] and *Dekens et al.* [2007] that an extensive part of the mid-Pliocene was characterized by protracted El Niño–like (El Padre) conditions.

[36] The termination of these conditions differs among the proxy records and among different EEP sites. At ODP Site 1241, TEX^{H}_{86} temperatures decrease from about 3.5 to 3 Ma, and productivity indicators increase at around 3 Ma. Adjusted Mg/Ca temperatures decrease from 4.0 to 2.5 Ma, but that is due almost entirely to the seawater Mg/Ca correction, and unadjusted Mg/Ca-derived temperatures exhibit no long-term change. The ODP Site 1241 productivity trends are similar in timing to those inferred from opal and alkenone MARs at ODP Site 846 and 847 [*Farrell et al.*, 1995; *Lawrence et al.*, 2006; *Dekens et al.*, 2007], although opal MARs at ODP Site 1239 suggest an earlier productivity increase at around 3.5 Ma [*Steph et al.*, 2010]. Further productivity increases at ODP Site 1241 (but not 847) occur between 2 and 1.5 Ma, broadly corresponding to the development of the $\Delta SST_{WEP\text{-}EEP}$ gradient based on Mg/Ca temperatures [*Wara et al.*, 2005]. Similar to the ODP Site 1241 diol records, dust inputs to the SE Pacific increase at 2.8 Ma and continue to gradually increase from 2 to 1.5 Ma [*Hovan*, 1995] (Figure 5d).

4.4. Causes of Observed Changes

[37] The causes of these changes remain the subject of debate. Previous workers have attributed changes in the thermal structure of the tropical Pacific water column to changes in ocean gateways, such as the closure of the Isthmus of Panama [*Haug and Tiedemann*, 1998; *Steph et al.*, 2010] and/or the reorganization of the Indonesian Throughflow [*Karas et al.*, 2009]. For example, it has been suggested that shoaling of the Isthmus of Panama gradually occurred during the Late Miocene with a dramatic shoaling at ~7 Ma and final closure occurring at about 2.7 Ma (see *Schmidt* [2007] for a review). This caused intensification of the Atlantic meridional overturning circulation (AMOC) from 4.7 to 4.2 Ma [*Huang et al.* 2000; *Steph et al.*, 2010], which in turn could have led to the globally warm conditions of the middle Pliocene, especially at higher latitudes [*Dowsett et al.*, 1996; *Klocker et al.*, 2005; *Lunt et al.*, 2008]. It could have also caused shoaling of the tropical Pacific thermocline to the deep photic zone as suggested by the *G. tumida* Mg/Ca temperatures at ODP Sites 1241 and 1239. However, the co-occurring increase in TEX^{H}_{86} temperatures and decrease in productivity indices suggests that such thermocline shoaling did not reach shallower depths. Our data indicate further shoaling of the thermocline above the base of photic zone at 3.5 Ma. Interestingly, the timing of the second shoaling is consistent with the reorganization of the Indonesian Gateway (3.5–3.0 Ma) [*Karas et al.*, 2009]. This may suggest that the tectonic reorganization of Indonesian Gateway could have contributed to the second shoaling of thermocline depth in EEP.

[38] A dramatic increase in ice rafted debris (IRD) occurred in the North Atlantic at 7 Ma (Figure 5f), indicating growth of the Greenland ice sheet to a size that allowed iceberg-carving in the Iceland-Norwegian Sea [*Fronval and Jansen*, 1996; *Lear et al.*, 2003]. Then at 2.8 Ma, the intensification of NHG (INHG) is clearly expressed by an increase in evidence for ice-rafted debris in the North Atlantic and Pacific Oceans, as well as a strong shift toward more positive values in benthic foraminiferal $\delta^{18}O$ values (Figures 5g and 5h). Both events occurred at or near the times of inferred diatom productivity increases (~7 Ma and ~3 Ma) at ODP Site 1241, and both could have been associated with an increased zonal temperature gradient, increased winds and increased upwelling intensity (e.g., Figure 5), providing a causative link between glaciation and upwelling. The cause of Northern hemisphere ice sheet growth remains unclear, but the expansion at 2.8 Ma has been attributed to a decline in pCO_2 [*Lunt et al.*, 2008; *Pagani et al.*, 2010; *Seki et al.*, 2010].

[39] Since the source of upwelled water in the tropics is subducted surface waters of the extratropic ocean [*Tsuchiya et al.*, 1989], colder SSTs at high latitudes also could have influenced tropical Pacific thermocline conditions [*Philander and Fedorov*, 2003; *Fedorov et al.*, 2006; *Brierley et al.*, 2009]. Like the closure of the Panama Seaway and restriction of Indonesian Throughflow, increased equator to pole temperature and/or salinity gradients can induce colder and/or shallower tropical thermoclines [*Boccaletti et al.*, 2004; *Fedorov et al.*, 2004]. In these models, a sufficiently shallow thermocline is a prerequisite for wind-induced upwelling to have a significant cooling effect on SSTs; under such conditions, ice volume-wind strength-upwelling feedbacks are enhanced, particularly in response to obliquity forcing. Thus, our long-term observations support arguments that a strong relationship between eastern tropical SST and high latitude climate existed long before 3 Ma [*Lawrence et al.*, 2006]. In order to evaluate climatic links between the tropics and extratropics in the late Miocene, longer-term SST records are required for the mid and high latitudes.

5. Conclusions

[40] We applied multiple geochemical proxies (Mg/Ca, $U^{K'}_{37}$ and TEX^{H}_{86} temperatures, MARs of algal biomarkers and diol indices) to ODP Site 1241 sediments in order to better

understand the long-term evolution of climate in the Eastern Tropical Pacific over the past 10 Myr. Sedimentary TEX_{86}^{H} temperatures at ODP Site 1241 appear to reflect subsurface thermocline temperatures rather than surface temperatures. Intriguingly, the long-term variability of TEX_{86}^{H} subsurface temperatures coincides well with *N. dutertrei* Mg/Ca temperatures that have been adjusted for putative changes in the Mg/Ca ratio of seawater [*Medina-Elizalde et al.*, 2008]. However, we stress that these (and similar) interpretations are highly contingent on the seawater Mg/Ca correction, for which there are only limited data; reproducing and expanding the temporal coverage of existing data is essential for future research. Alternatively, the TEX_{86}^{H} temperature record could be explained by changes in the depth from which GDGTs are exported, and this also would reflect changes in the EEP paleoceanography.

[41] TEX_{86}^{H} temperatures at ODP Site 1241 exhibit a long-term decrease over the past 10 Myr, interrupted by apparent warming from 5.5 to 4.5 Ma. Combined with productivity records (phytoplankton biomarker fluxes and diol indices), they suggest that in the EEP, protracted El Niño–like conditions prevailed during the Pliocene (5.5–3 Ma), as indicated by previous studies, but also prior to 7 Ma. Moderate La Niña conditions prevailed from 7 to 4.5 Ma, corresponding to the late Miocene global cooling. Overall, these long-term records offer further evidence that the upwelling regime in the EEP is strongly linked to long-term global climate change, potentially to pCO_2 levels via their impact on NHG.

[42] **Acknowledgments.** This research used samples provided by the Ocean Drilling Program (ODP). ODP is sponsored by the U.S. National Science Foundation (NSF) and participating countries under management of Joint Oceanographic Institutions (JOI), Inc. O.S. acknowledges the support by Japan Society of Promotion of Science funded by Ministry of Education, Culture, Sports, Science and Technology, Japan. D.N.S. acknowledges support from the Royal Society in the form of University Research Fellowship. R.D.P. acknowledges analytical support from the Bristol Node of the NERC Life Sciences Mass Spectrometry Facility. S.S. acknowledges support from the Netherlands Organisation for Scientific Research (NWO) in the form of a VICI grant. We are very grateful to three anonymous reviewers and the associate editor for constructive comments.

References

Anand, P., H. Elderfield, and M. Conte (2003), Calibration of Mg/Ca thermometry in planktonicforaminifera from a sediment trap time series, *Paleoceanography*, *18*(2), 1050, doi:10.1029/2002PA000846.

Bartoli, G., M. Sarnthein, M. Weinelt, H. Erlenkeuser, D. Garbe-Schonberg, and D. Lea (2005), Final closure of Panama and the onset of Northern Hemisphere glaciation, *Earth Planet. Sci. Lett.*, *237*, 33–44, doi:10.1016/j.epsl.2005.06.020.

Bickert, T., G. H. Haug, and R. Tiedemann (2004), Late Neogene benthic stable isotope record of Ocean Drilling Program Site 999: Implications for Caribbean paleoceanography, organic carbon burial, and the Messinian Salinity Crisis, *Paleoceanography*, *19*, PA1023, doi:10.1029/2002PA000799.

Boccaletti, G., R. C. Pacanowski, S. G. H. Philander, and A. V. Fedorov (2004), The thermal structure of the upper ocean, *J. Phys. Oceanogr.*, *34*, 888–902, doi:10.1175/1520-0485(2004)034<0888:TTSOTU>2.0.CO;2.

Brierley, C. M., A. V. Fedorov, Z. Liu, T. D. Herbert, K. T. Lawrence, and J. P. LaRriviere (2009), Greatly expanded tropical warm pool and weakened Hadley circulation in the early Pliocene, *Science*, *323*, 1714–1718, doi:10.1126/science.1167625.

Cane, M. A. (1998), A role for the Tropical Pacific, *Science*, *282*, 59–61, doi:10.1126/science.282.5386.59.

Coggon, R. M., D. A. H. Teagle, C. E. Smith-Duque, J. C. Alt, and M. J. Cooper (2010), Reconstructing past seawater Mg/Ca and Sr/Ca from mid-ocean ridge flank calcium carbonate veins, *Science*, *327*, 1114–1117, doi:10.1126/science.1182252.

Conte, M. H., J. K. Volkman, and G. Engliton (1994), Lipid biomarkers of the Haptophyta, in *The Haptophyte Algae*, edited by J. C. Green et al., pp. 351–377, Clarendon Univ. Press, Oxford, U. K.

Conte, M. H., M. A. Sicre, C. Ruehlemann, J. C. Weber, S. Schulte, D. Schulz-Bull, and T. Blanz (2006), Global temperature calibration of the alkenone unsaturation index ($U_{37}^{K'}$) in surface waters and comparison with surface sediments, *Geochem. Geophys. Geosyst.*, *7*, Q02005, doi:10.1029/2005GC001054.

Dekens, P. S., D. W. Lea, D. K. Pak, and H. J. Spero (2002), Core top calibration of Mg/Ca in tropical foraminifera: Refining paleotemperature estimation, *Geochem. Geophys. Geosyst.*, *3*(4), 1022, doi:10.1029/2001GC000200.

Dekens, P. S., A. C. Ravelo, and M. D. McCarthy (2007), Warm upwelling regions in the Pliocene warm period, *Paleoceanography*, *22*, PA3211, doi:10.1029/2006PA001394.

de la Torre, J. R., C. B. Walker, A. E. Ingalls, M. Könneke, and D. A. Stahl (2008), Cultivation of a thermophilic ammonia oxidizing archaeon synthesizing crenarchaeol, *Environ. Microbiol.*, *10*, 810–818, doi:10.1111/j.1462-2920.2007.01506.x.

Diester-Haass, L., K. Billups, and K. C. Emeis (2006), Late Miocene carbon isotope records and marine biological productivity: Was there a (dusty) link?, *Paleoceanography*, *21*, PA4216, doi:10.1029/2006PA001267.

Dowsett, H., J. Barron, and R. Poore (1996), Middle Pliocene sea surface temperatures: A global reconstruction, *Mar. Micropaleontol.*, *27*, 13–25, doi:10.1016/0377-8398(95)00050-X.

Fairbanks, R. G., M. Sverdlove, R. Free, P. H. Wiebe, and A. W. H. Bé (1982), Vertical distribution and isotopic fractionation of living planktonic foraminifera from the Panama Basin, *Nature*, *298*, 841–844, doi:10.1038/298841a0.

Fantle, M. S., and D. J. DePaolo (2005), Variations in the marine Ca cycle over the past 20 million years, *Earth Planet. Sci. Lett.*, *237*, 102–117, doi:10.1016/j.epsl.2005.06.024.

Fantle, M. S., and D. J. DePaolo (2006), Sr isotopes and pore fluid chemistry in carbonate sediment of the Ontong Java Plateau: Calcite recrystallization rates and evidence for a rapid rise in seawater Mg over the last 10 million years, *Geochim. Cosmochim. Acta*, *70*, 3883–3904, doi:10.1016/j.gca.2006.06.009.

Fantle, M. S., and D. J. DePaolo (2007), Ca isotopes in carbonate sediment and pore fluid from ODP Site 807A: The Ca^{2+}(aq)–calcite equilibrium fractionation factor and calcite recrystallization rates in Pleistocene sediments, *Geochim. Cosmochim. Acta*, *71*, 2524–2546, doi:10.1016/j.gca.2007.03.006.

Farrell, J. W., et al. (1995), Late Neogene sedimentation patterns in the eastern equatorial Pacific Ocean, *Proc. Ocean Drill. Program Sci. Results*, *138*, 717–756.

Fedorov, A. V., R. C. Pacanowski, S. G. Philander, and G. Boccaletti (2004), The effect of salinity on the wind-driven circulation and the thermal structure of the upper ocean, *J. Phys. Oceanogr.*, *34*, 1949–1966, doi:10.1175/1520-0485(2004)034<1949:TEOSOT>2.0.CO;2.

Fedorov, A. V., P. S. Dekens, M. McCarthy, A. C. Ravelo, P. B. deMenocal, M. Barreiro, R. C. Pacanowski, and S. G. Philander (2006), The Pliocene Paradox (Mechanisms for a Permanent El Niño), *Science*, *312*, 1485–1489, doi:10.1126/science.1122666.

Flores, J.-A., W. Wei, G. E. López-Otálvaro, C. Alvarez, and F. J. Sierro (2006), Tropical and Equatorial calcareous nannofossil Pleistocene biostratigraphy, *Proc. Ocean Drill. Program Sci. Results*, *202*, 10 pp., doi:10.2973/odp.proc.sr.202.214.2006.

Fronval, T., and E. Jansen (1996), Late Neogene paleoclimates and paleoceanography in the Iceland-Norwegian Sea: Evidence from the Iceland and Vøring Plateaus, *Proc. Ocean Drill. Program Sci. Results*, *151*, 455–468.

Griffith, E. M., A. Paytan, K. Caldeira, T. D. Bullen, and E. Thomas (2008), A dynamic marine calcium cycle during the past 28 million years, *Science*, *322*, 1671–1674, doi:10.1126/science.1163614.

Groeneveld, J., S. Steph, R. Tiedemann, D. Garbe-Schönberg, D. Nürnberg, and A. Sturm (2006), Pliocene mixed-layer oceanography for site 1241, using combined Mg/Ca and $\delta^{18}O$ analyses of *Globigerinoides sacculifer*, *Proc. Ocean Drill. Program Sci. Results*, *202*, 27 pp., doi:10.2973/odp.proc.sr.202.209.2006.

Haug, G. H., and R. Tiedemann (1998), Effect of the formation of the Isthmus of Panama on Atlantic Ocean thermohaline circulation, *Nature*, *393*, 673–676, doi:10.1038/31447.

Haug, G. H., M. A. Maslin, M. Sarnthein, R. Stax, and R. Tiedemann (1995), Evolution of Northwest Pacific sedimentation patterns since 6 Ma (site 882), *Proc. Ocean Drill. Program Sci. Results*, *145*, 293–314.

Haywood, A. M., and P. J. Valdes (2004), Modelling Pliocene warmth: Contribution of atmosphere, oceans and cryosphere, *Earth Planet. Sci. Lett.*, *218*, 363–377, doi:10.1016/S0012-821X(03)00685-X.

Haywood, A. M., P. Dekens, A. C. Ravelo, and M. Pagani (2005), Warmer tropics during the mid-Pliocene? Evidence from alkenone paleothermometry

and a fully coupled ocean-atmosphere GCM, *Geochem. Geophys. Geosyst.*, *6*, Q03010, doi:10.1029/2004GC000799.

Haywood, A. M., P. J. Valdes, and V. L. Peck (2007), A permanent El Niño-like state during the Pliocene?, *Paleoceanography*, *22*, PA1213, doi:10.1029/2006PA001323.

Heuser, A., A. Eisenhauer, F. Böhm, K. Wallmann, N. Gussone, P. N. Pearson, T. F. Nägler, and W.-C. Dullo (2005), Calcium isotope ($\delta^{44/40}$Ca) variations of Neogene planktonic foraminifera, *Paleoceanography*, *20*, PA2013, doi:10.1029/2004PA001048.

Ho, S. L., M. Yamamoto, G. Mollenhauer, and M. Minagawa (2011), Core top TEX_{86} values in the south and equatorial Pacific, *Org. Geochem.*, *42*, 94–99, doi:10.1016/j.orggeochem.2010.10.012.

Hopmans, E. C., J. W. H. Weijers, E. Schefuß, L. Herfort, J. S. Sinninghe Damsté, and S. Schouten (2004), A novel proxy for terrestrial organic matter in sediments based on branched and isoprenoid tetraether lipids, *Earth Planet. Sci. Lett.*, *224*, 107–116, doi:10.1016/j.epsl.2004.05.012.

Horita, J., H. Zimmermann, and F. D. Holland (2002), Chemical evolution of seawater during the Phanerozoic: Implications from the records of marine evaporates, *Geochim. Cosmochim. Acta*, *66*, 3733–3756, doi:10.1016/S0016-7037(01)00884-5.

Hovan, S. A. (1995), Late Cenozoic atmospheric circulation intensity and climatic history recorded by eolian deposition in the eastern equatorial Pacific Ocean, Leg 138, *Proc. Ocean Drill. Program Sci. Results*, *138*, 615–625.

Huang, R. X., M. A. Cane, N. Naik, and P. Goodman (2000), Global adjustment of the thermocline in response to deepwater formation, *Geophys. Res. Lett.*, *27*, 759–762, doi:10.1029/1999GL002365.

Huguet, C., A. Schimmelmann, R. Thunell, L. J. Lourens, J. S. Sinninghe Damsté, and S. Schouten (2007), A study of the TEX_{86} paleothermometer in the water column and sediments of the Santa Barbara Basin, California, *Paleoceanography*, *22*, PA3203, doi:10.1029/2006PA001310.

Karas, C., D. Nürnberg, A. K. Gupta, R. Tiedemann, and K. Mohan (2009), Mid-Pliocene climate change amplified by a switch in Indonedian subsurface throughflow, *Nat. Geosci.*, *2*, 434–438, doi:10.1038/ngeo520.

Karner, M. B., E. F. DeLong, and D. M. Karl (2001), Archaeal dominance in the mesopelagic zone of the Pacific Ocean, *Nature*, *409*, 507–510, doi:10.1038/35054051.

Kim, J.-H., J. van der Meer, S. Schouten, P. Helmke, V. Willmott, F. Sangiorgi, N. Koç, E. C. Hopmans, and J. S. Sinninghe Damsté (2010), New indices and calibrations derived from the distribution of crenarchaeal isoprenoid tetraether lipids: Implications for past sea surface temperature reconstructions, *Geochim. Cosmochim. Acta*, *74*, 4639–4654, doi:10.1016/j.gca.2010.05.027.

Klocker, A., M. Prange, and M. Schulz (2005), Testing the influence of the Central American Seaway on orbitally forced Northern Hemisphere glaciation, *Geophys. Res. Lett.*, *32*, L03703, doi:10.1029/2004GL021564.

Koning, E., J. M. Van Iperen, W. Van Raaphorst, W. Helder, G.-J. A. Brummer, and T. C. E. van Weering (2001), Selective preservation of upwelling-indicating diatoms in sediments off Somalia, NW Indian Ocean, *Deep Sea Res., Part I*, *48*, 2473–2495, doi:10.1016/S0967-0637(01)00019-X.

Könneke, M., A. E. Bernhard, J. R. de la Torre, C. B. Walker, J. B. Waterbury, and D. A. Stahl (2005), Isolation of an autotrophic ammonia-oxidizing marine archaeon, *Nature*, *437*, 543–546, doi:10.1038/nature03911.

Lawrence, K. T., Z. Liu, and T. D. Herbert (2006), Evolution of the eastern tropical Pacific through Plio-Pleistocene glaciation, *Science*, *312*, 79–83, doi:10.1126/science.1120395.

Lawrence, K. T., T. D. Herbert, C. M. Brown, M. E. Raymo, and A. M. Haywood (2009), High-amplitude variation in North Atlantic sea surface temperature during the early Pliocene warm period, *Paleoceanography*, *24*, PA2218, doi:10.1029/2008PA001669.

Lear, C. H., Y. Rosenthal, and J. D. Wright (2003), The closing of a seaway: Ocean water masses and global climate change, *Earth Planet. Sci. Lett.*, *210*, 425–436, doi:10.1016/S0012-821X(03)00164-X.

Lee, K. E., J.-H. Kim, I. Wilke, P. Helmke, and S. Schouten (2008), A study of the alkenone, TEX_{86}, and planktonic foraminifera in the Benguela Upwelling System: Implications for past sea surface temperature estimates, *Geochem. Geophys. Geosyst.*, *9*, Q10019, doi:10.1029/2008GC002056.

Lisiecki, L. E., and M. E. Raymo (2005), A Pliocene-Pleistocene stack of 57 globally distributed benthic δ^{18}O records, *Paleoceanography*, *20*, PA1003, doi:10.1029/2004PA001071.

Locarnini, R. A., A. V. Mishonov, J. I. Antonov, T. P. Boyer, and H. E. Garcia (2006), *World Ocean Atlas 2005*, vol. 1, *Temperature*, *NOAA Atlas NESDIS*, vol. 61, edited by S. Levitus, 182 pp., NOAA, Silver Spring, Md.

Lopes dos Santos, R. A., M. Prange, I. S. Castañeda, E. Schefuß, S. Mulitza, M. Schulz, E. M. Niedermeyer, J. S. Sinninghe Damsté, and S. Schouten (2010), Glacial–interglacial variability in Atlantic meridional overturning circulation and thermocline adjustments in the tropical North Atlantic, *Earth Planet. Sci. Lett.*, *300*, 407–414, doi:10.1016/j.epsl.2010.10.030.

Lowenstein, T. M., M. N. Timofeeff, S. T. Brennan, L. A. Hardie, and R. V. Democco (2001), Oscillations in Phanerozoic seawater chemistry: Evidence from fluid inclusions, *Science*, *294*, 1086–1088, doi:10.1126/science.1064280.

Lunt, D. J., G. L. Foster, A. M. Haywood, and E. J. Stone (2008), Late Pliocene Greenland glaciation controlled by a decline in atmospheric CO_2 levels, *Nature*, *454*, 1102–1105, doi:10.1038/nature07223.

Lunt, D. J., A. M. Haywood, G. A. Schmidt, U. Salzmann, P. J. Valdes, and H. J. Dowsett (2010), Earth system sensitivity inderred from Pliocene modeling and data, *Nat. Geosci.*, *3*, 60–64, doi:10.1038/ngeo706.

Margalef, R. (1978), Life-forms of phytoplankton as survival alternatives in an unstable environment, *Oceanol. Acta*, *1*, 493–509.

Medina-Elizalde, M., and D. W. Lea (2010), Late Pliocene equatorial Pacific, *Paleoceanography*, *25*, PA2208, doi:10.1029/2009PA001780.

Medina-Elizalde, M., D. W. Lea, and M. S. Fantle (2008), Implications of seawater Mg/Ca variability for Plio-Pleistocene tropical climate reconstruction, *Earth Planet. Sci. Lett.*, *269*, 585–595, doi:10.1016/j.epsl.2008.03.014.

Meehl, G. A., et al. (2007), Global climate projections, in *Climate Change 2007: The Physical Science Basis: Contribution of Working Group I to the Fourth Assessment Report on the Intergovernmental Panel on Climate Change*, edited by S. Solomon et al., pp. 747–845, Cambridge Univ. Press, Cambridge, U. K.

Méjanelle, L., A. Sanchez-Gargallo, I. Bentaleb, and J. O. Grimalt (2003), Long chain n-alkyl diols, hydroxy ketones and sterols in a marine eustigmatophyte, Nannochloropsis gaditana, and in Brachionus plicatilis feeding on the algae, *Org. Geochem.*, *34*, 527–538, doi:10.1016/S0146-6380(02)00246-2.

Mix, A. C., et al. (2003), Chapter 12, Site 1241, *Proc. Ocean Drill. Program Initial Rep.*, *202*, 101 pp., doi:10.2973/odp.proc.ir.202.112.2003.

Moore, J. K., S. C. Doney, and K. Lindsay (2004), Upper ocean ecosystem dynamics and iron cycling in a global three-dimensional model, *Global Biogeochem. Cycles*, *18*, GB4028, doi:10.1029/2004GB002220.

Mucci, A., and J. W. Morse (1983), The incorporation of Mg^{2+} and Sr^{2+} into calcite overgrowths: Influences of growth rate and solution composition, *Geochim. Cosmochim. Acta*, *47*, 217–233, doi:10.1016/0016-7037(83)90135-7.

Müller, P. J., O. Kirst, G. Ruhiand, I. V. Storch, and A. Rosell-Melé (1998), Calibration of alkenone paleotemperature index $U^{K'}_{37}$ based on core-tops from the eastern South Atlantic and the global ocean (60°N–60°S), *Geochim. Cosmochim. Acta*, *62*, 1757–1772, doi:10.1016/S0016-7037(98)00097-0.

Nathan, S. A., and R. M. Leckie (2009), Early history of the Western Pacific Warm Pool during the middle to late Miocene (~13.2–5.8 Ma): Role of sea-level change and implications for equatorial circulation, *Palaeogeogr. Palaeoclimatol. Palaeoecol.*, *274*, 140–159, doi:10.1016/j.palaeo.2009.01.007.

Pagani, M., Z. Liu, J. LaRiviere, and A. C. Ravelo (2010), High Earth-system climate sensitivity determined from Pliocene carbon dioxide concentrations, *Nat. Geosci.*, *3*, 27–30, doi:10.1038/ngeo724.

Philander, S. G., and A. V. Fedorov (2003), Role of tropics in changing the response to Milankovich forcing some three million years ago, *Paleoceanography*, *18*(2), 1045, doi:10.1029/2002PA000837.

Pitcher, A., N. Rychlik, E. C. Hopmans, E. Spieck, W. I. C. Rijpstra, J. Ossebaar, S. Schouten, M. Wagner, and J. S. Sinninghe Damsté (2010), Crenarchaeol dominates the membrane lipids of Candidatus Nitrososphaera gargensis, a thermophilic Group I.1b Archaeon, *ISME J.*, *4*, 542–552, doi:10.1038/ismej.2009.138.

Prahl, F. G., A. C. Mix, and M. A. Sparrow (2006), Alkenone paleothermometry: Biological lessons from marine sediment records off western South America, *Geochim. Cosmochim. Acta*, *70*, 101–117, doi:10.1016/j.gca.2005.08.023.

Rampen, S. W., S. Schouten, S. G. Wakeham, and J. S. Sinninghe Damsté (2007), Seasonal and spatial variation in the sources and fluxes of long chain diols and mid-chain hydroxy methyl alkenoates in the Arabian Sea, *Org. Geochem.*, *38*, 165–179, doi:10.1016/j.orggeochem.2006.10.008.

Rampen, S. W., S. Schouten, G. J. Brummer, E. Koning, and J. S. Sinninghe Damsté (2008), A 90 ka upwelling record from the northwestern Indian Ocean using a novel long-chain diol index, *Earth Planet. Sci. Lett.*, *276*, 207–213, doi:10.1016/j.epsl.2008.09.022.

Rampen, S. W., S. Schouten, and J. S. Sinninghe Damsté (2011), Occurrence of long chain 1,14-diols in *Apedinella radians*, *Org. Geochem.*, *42*, 572–574, doi:10.1016/j.orggeochem.2011.03.009.

Ravelo, A. C., and R. G. Fairbanks (1992), Oxygen isotopic composition of multiple species of planktonic foraminifera: Recorders of the modern photic zone temperature gradient, *Paleoceanography*, *7*, 815–831, doi:10.1029/92PA02092.

Ravelo, A. C., D. H. Andreasen, M. Lyle, A. O. Lyle, and M. W. Wara (2004), Regional climate shifts caused by gradual global cooling in the Pliocene, *Nature*, *429*, 263–267, doi:10.1038/nature02567.

Ravelo, A. C., P. S. Dekens, and M. McCarthy (2006), Evidence for El Niño like conditions during the Pliocene, *GSA Today*, *16*, 4–11, doi:10.1130/1052-5173(2006)016<4:EFENLC>2.0.CO;2.

Rea, D. K. (1994), The paleoclimatic record provided by eolian deposition in the deep-sea: The geologic history of wind, *Rev. Geophys.*, *32*, 159–195, doi:10.1029/93RG03257.

Rea, D. K., H. Snoeckx, and L. H. Joseph (1998), Late Cenozoic eolian deposition in the North Pacific: Asian drying, Tibetian uplift, and cooling of the Northern Hemisphere, *Paleoceanography*, *13*, 215–224, doi:10.1029/98PA00123.

Rickaby, R. E. M., and P. Halloran (2005), Cool La Niña during the warmth of the Pliocene?, *Science*, *307*, 1948–1952, doi:10.1126/science.1104666.

Schmidt, D. N. (2007), The closure history of the Central American seaway: Evidence from isotopes and fossils to models and molecules, in *Deep-Time Perspectives on Climate Change: Marrying the Signal from Computer Models and Biological Proxies*, edited by M. Williams et al., pp. 427–442, Geol. Soc., London.

Schouten, S., E. C. Hopmans, E. Schefub, and J. S. Sinninghe Damsté (2002), Distributional variations in marine crenarchaeotal membrane lipids: A new tool for reconstructing ancient sea water temperatures?, *Earth Planet. Sci. Lett.*, *204*, 265–274, doi:10.1016/S0012-821X(02)00979-2.

Schouten, S., C. Huguet, E. C. Hopmans, and J. S. Sinninghe Damsté (2007), Analytical methodology for TEX_{86} paleothermometry by high-performance liquid chromatography/atmospheric pressure chemical ionization-mass spectrometry, *Anal. Chem.*, *79*, 2940–2944, doi:10.1021/ac062339v.

Schouten, S., E. C. Hopmans, M. Baas, H. Boumann, S. Standfest, M. Könneke, D. A. Stahl, and J. S. Sinninghe Damsté (2008), Intact membrane lipids of *Candidatus* "Nitrosopumilus maritimus", a cultivated representative of the cosmopolitan mesophilic Group I Crenarchaeota, *Appl. Environ. Microbiol.*, *74*, 2433–2440, doi:10.1128/AEM.01709-07.

Seki, O., M. Ikehara, K. Kawamura, T. Nakatsuka, K. Ohnishi, M. Wakatsuchi, H. Narita, and T. Sakamoto (2004), Reconstruction of paleoproductivity in the Sea of Okhotsk over the last 30 kyr, *Paleoceanography*, *19*, PA1016, doi:10.1029/2002PA000808.

Seki, O., G. L. Foster, D. N. Schmidt, A. Mackensen, K. Kawamura, and R. D. Pancost (2010), Alkenone and boron-based Pliocene pCO_2 records, *Earth Planet. Sci. Lett.*, *292*, 201–211, doi:10.1016/j.epsl.2010.01.037.

Sime, N. G., C. L. De La Rocha, E. T. Tipper, A. Tripati, A. Galy, and M. J. Bickle (2007), Interpreting the Ca isotope record of marine biogenic carbonates, *Geochim. Cosmochim. Acta*, *71*, 3979–3989, doi:10.1016/j.gca.2007.06.009.

Sinninghe Damsté, J. S., et al. (2003), Diatomaceous origin for long-chain diols and mid-chain hydroxy methyl alkanoates widely occurring in Quaternary marine sediments: Indicators for high-nutrient conditions, *Geochim. Cosmochim. Acta*, *67*, 1339–1348, doi:10.1016/S0016-7037(02)01225-5.

Sonzogni, C., E. Bard, F. Rostek, R. Lafont, A. Rosell-Mele, and G. Eglinton (1997), Core-top calibration of the alkenone index vs sea surface temperature in the Indian Ocean, *Deep Sea Res., Part II*, *44*, 1445–1460, doi:10.1016/S0967-0645(97)00010-6.

Stanley, S. M., and L. A. Hardie (1998), Secular oscillations in the carbonate mineralogy of reef-building and sediment-producing organisms driven by techtonically forced shifts in seawater chemistry, *Palaeogeogr. Palaeoclimatol. Palaeoecol.*, *144*, 3–19, doi:10.1016/S0031-0182(98)00109-6.

Steph, S., R. Tiedemann, J. Groeneveld, A. Sturm, and D. Nürngerg (2006), Pliocene changes in Tropical East Pacific upper ocean stratification, Response to Tropical Gateways?, *Proc. Ocean Drill. Program Sci. Results*, *202*, 51 pp., doi:10.2973/odp.proc.sr.202.211.2006.

Steph, S., R. Tiedemann, M. Prange, J. Groeneveld, M. Schulz, A. Timmermann, D. Nürnberg, C. Rühlemann, C. Saukel, and G. H. Haug (2010), Early Pliocene increase in thermohaline overturning: A precondition for the development of the modern equatorial Pacific cold tongue, *Paleoceanography*, *25*, PA2202, doi:10.1029/2008PA001645.

Thiede, J., et al. (1998), Late Cenozoic history of the polar North Atlantic: Results from ocean drilling, *Quat. Sci. Rev.*, *17*, 185–208, doi:10.1016/S0277-3791(97)00076-0.

Tiedemann, R., A. Sturm, S. Steph, S. P. Lund, and J. S. Stoner (2006), Astronomically calibrated timescales from 6 to 2.5 Ma and benthic isotope stratigraphies, sites 1236, 1237, 1239 and 1241, *Proc. Ocean Drill. Program Sci. Results*, *202*, 69 pp., doi:10.2973/odp.proc.sr.202.210.2007.

Tsuchiya, M., R. Lukas, R. A. Fine, E. Firing, and E. Lindstrom (1989), Source waters of the Pacific Equatorial Undercurrent, *Prog. Oceanogr.*, *23*, 101–147, doi:10.1016/0079-6611(89)90012-8.

Vidal, L., T. Bickert, G. Wefer, and U. Röhl (2002), Late Miocene stable isotope stratigraphy of SE Atlantic ODP Site 1085: Relation to Messinian events, *Mar. Geol.*, *180*, 71–85, doi:10.1016/S0025-3227(01)00206-7.

Volkman, J. K., S. M. Barrett, G. A. Dunstan, and S. W. Jeffrey (1992), C30-C32 alkyl diols and unsaturated alcohols in microalgae of the class Eustigmatophyceae, *Org. Geochem.*, *18*, 131–138, doi:10.1016/0146-6380(92)90150-V.

Wang, C., and P. C. Fiedler (2006), ENSO variability and the eastern tropical Pacific: A review, *Prog. Oceanogr.*, *69*, 239–266, doi:10.1016/j.pocean.2006.03.004.

Wara, M. W., A. C. Ravelo, and M. L. Delaney (2005), Permanent El Niño like conditions during the Pliocene warm period, *Science*, *309*, 758–761, doi:10.1126/science.1112596.

Weijers, J. W. H., S. Schouten, O. C. Spaargaren, and J. S. Sinninghe Damsté (2006), Occurrence and distribution of tetraether membrane lipids in soils: Implications for the use of the TEX_{86} proxy and the BIT index, *Org. Geochem.*, *37*, 1680–1693, doi:10.1016/j.orggeochem.2006.07.018.

Wilkinson, B. H., and T. J. Algeo (1989), Sedimentary carbonate record of calcium–magnesium cycling, *Am. J. Sci.*, *289*, 1158–1194, doi:10.2475/ajs.289.10.1158.

Wuchter, C., et al. (2006), Archaeal nitrification in the ocean, *Proc. Natl. Acad. Sci. U. S. A.*, *103*, 12,317–12,322, doi:10.1073/pnas.0600756103.

Ziveri, P., and R. C. Thunell (2000), Coccolithophore export production in Guaymas Basin, Gulf of California: Response to climate forcing, *Deep Sea Res., Part II*, *47*, 2073–2100, doi:10.1016/S0967-0645(00)00017-5.